PImMS, a fast event-triggered monolithic pixel detector with storage of multiple timestamps

2012 JINST 7 C08001

(http://iopscience.iop.org/1748-0221/7/08/C08001)

PUBLISHED BY IOP PUBLISHING FOR SISSA MEDIALAB

RECEIVED: *May 10, 2012*
ACCEPTED: *July 9, 2012*
PUBLISHED: *August 16, 2012*

THE 9th INTERNATIONAL CONFERENCE ON POSITION SENSITIVE DETECTORS,
12–16 SEPTEMBER 2011,
ABERYSTWYTH, U.K.

PImMS, a fast event-triggered monolithic pixel detector with storage of multiple timestamps

J.J. John,[1a] **M. Brouard,**[b] **A. Clark,**[d] **J. Crooks,**[d] **E. Halford,**[b] **L. Hill**[a] **J.W.L. Lee,**[c] **A. Nomerotski**[a] **R. Pisarczyk,**[a] **I. Sedgwick,**[d] **C.S. Slater,**[b] **R. Turchetta,**[d] **C. Vallance,**[c] **E. Wilman,**[c] **B. Winter**[b] **and W.H. Yuen**[b]

[a] *Department of Physics, Oxford University, Oxford, OX1 3RH, United Kingdom*
[b] *The Physical and Theoretical Chemistry Laboratory, Department of Chemistry, Oxford University, Oxford, OX1 3QZ, United Kingdom*
[c] *Chemistry Research Laboratory, Department of Chemistry, Oxford University, 12 Mansfield Road, Oxford, OX1 3TA, United Kingdom*
[d] *Rutherford Appleton Laboratory, Science and Technology Facilities Council (STFC), Didcot, OX11 0QX, United Kingdom*

E-mail: Jaya.John@physics.ox.ac.uk

ABSTRACT: PImMS, or Pixel Imaging Mass Spectrometry, is a novel high-speed monolithic CMOS imaging sensor tailored to mass spectrometry requirements, also suitable for other dark-field applications. In its application to time-of-flight mass spectrometry, the sensor permits ion arrival time distributions to be combined with 2D imaging, providing additional information about the initial position or velocity of ions under study. PImMS1, the first generation sensor in this family, comprises an array of 72 by 72 pixels on a 70 μm by 70 μm pitch. Pixels independently record digital timestamps when events occur over an adjustable threshold. Each pixel contains 4 memories to record timestamps at a resolution of 25 ns. The sensor was designed and manufactured in the INMAPS 0.18 μm process. This allows the inclusion of significant amounts of circuitry (over 600 transistors) within each pixel while maintaining good detection efficiency. We present an overview of the pixel and sensor architecture, explain its functioning and present test results, ranging from characterisation of the analogue front end of the pixel, to verification of its digital functions, to some first images captured on mass spectrometers. We conclude with an overview of the upcoming second generation of PImMS sensors.

KEYWORDS: VLSI circuits; Mass spectrometers; Instrumentation and methods for time-of-flight (TOF) spectroscopy; Ion identification systems

[1] Corresponding author.

doi:10.1088/1748-0221/7/08/C08001

Contents

2012 JINST 7 C08001

1 Introduction

Time-of-flight mass spectrometry (TOF-MS) is a widely-used chemical analysis technique. Neutral sample molecules are ionized, often leading to fragmentation, and the resulting parent and fragment ions are accelerated by an electrostatic field along a flight tube to a time-resolved detector. Each ion acquires the same kinetic energy in the field, with the result that ions of different mass fly at different velocities and are separated in time at the detector. In ion imaging, further information is gained by employing a position sensitive detector to record the position of arriving ions on an image plane perpendicular to the flight path [1]–[3]. Figure 1 shows a schematic of a typical velocity-map ion imaging instrument. Typically, the ion flight times span a range from tens to hundreds of microseconds. The time resolution requirements depend on the desired mass resolution, and range from around 0.1 ns in state-of-the-art time-of-flight mass spectrometers to over 100 ns in a velocity-map imaging instrument designed to study small molecule fragmentation dynamics.

The position sensitive detectors used in imaging mass spectrometry generally employ one or two stacked microchannel plates (MCPs), usually coupled to a phosphor screen/camera combination. MCPs are thin resistively-coated glass plates incorporating a regular array of micron-sized holes. An ion striking the front face of the plate generates an electron cascade through one of

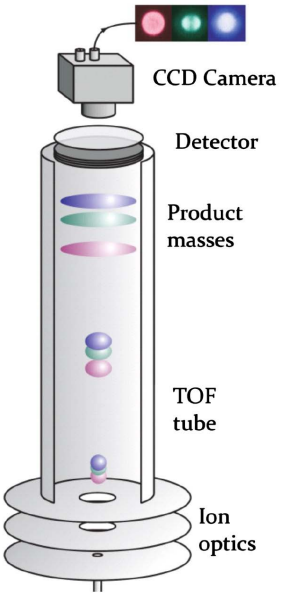

Figure 1. Schematic view of an ion imaging apparatus.

the channels, leading to a burst of electrons from the back face of the plate. These electrons are accelerated towards a phosphor screen, producing a flash of light that may be captured by a camera.

Until recently, limits on image transfer rates meant that only a single ion mass could be recorded on each time-of-flight cycle of an experiment, with mass selection achieved through time-gating either of the MCP or of an intensifier positioned in front of the camera. Multiple iterations of the image acquisition procedure were therefore required in order to obtain a complete set of images for all fragment ions. Advances in silicon detector technologies have now enabled the imaging of multiple masses per iteration. We have demonstrated this approach, Pixel Imaging Mass Spectrometry (PImMS) [4], in proof-of-principle experiments using both CCD and CMOS imaging sensors [5, 6].

When imaging with significant ambient light backgrounds (bright-field imaging), where the goal is generally to read out every frame acquired by the sensor, there is a trade-off between readout speed and the number of frames which can be read in a burst. The sensors with a high readout rate tend to have a limit on how many frames can be stored and then read out at that rate [7].

For imaging applications in which relatively few bright events are expected against a dark background (dark-field imaging), as in many mass spectrometry techniques, it is feasible and useful to sparsify images to reduce the volume of data to be read out. Using the approach of time-stamping significant events, the PImMS collaboration has specified and designed a custom CMOS imaging sensor for mass spectrometry and allied fields, known as the PImMS1 sensor.

2 PImMS1 sensor specifications

2.1 Pixel design

The resulting PImMS sensor addresses many of the technological requirements for TOF-MS outlined above. Each PImMS pixel is designed to act as an independent mass spectrometer, recording up to four significant events as digital timecodes.

2012 JINST 7 C08001

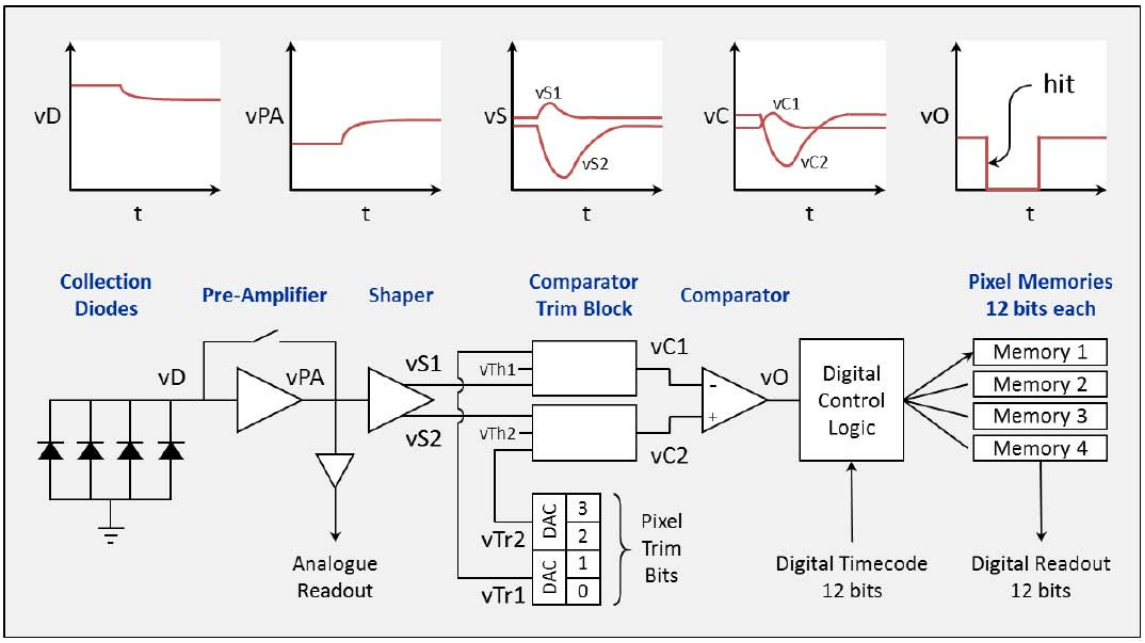

Figure 2. PImMS1 pixel schematics including intermediate signals.

As shown in the pixel schematics in figure 2, the pixel operates as follows: detection of light is accomplished by 4 photodiodes tied together (see the plot for the diode voltage vD). The signal on the charge collection node is first amplified by an integrating pre-amplifier (see plot for the pre-amplifier output voltage vPA), then a CR-RC shaper produces two pulses which represent the hit size in differential form (see the plot for the shaper outputs vS1 and vS2). The pulses are thresholded and trimmed by the comparator trim block which will be further described below (see the plot for the comparator inputs vC1 and vC2). Next the comparator evaluates whether a hit above the pixel's threshold has taken place, signalling hits to the digital controller (see the plot for the comparator output vO). When a hit occurs, the digital controller stores the current value of the global 12-bit timecode into one of four inbuilt 12-bit registers, recording ion arrival times with up to 25 ns timing precision. The 12-bit timecode permits dividing the experimental period into 4095 equal time slices.

It is worth noting that the shaper functions as a high-pass filter, passing only step changes in the diode charge, reducing noise at the comparator and removing slow-changing components such as the leakage current.

Event thresholding functions as follows: each pixel receives a pair of global DC bias voltages, indicated as vTh1 and vTh2 in figure 2. Their difference (vTh1 − vTh2) sets the event threshold for all pixels. In addition, each pixel contains a 4-bit trim register. The trim register configures two in-pixel DACs, generating local adjustment voltages shown as vTr1 and vTr2 in figure 2. This allows an individual adjustment to the threshold voltage used in each pixel, to compensate for process variations which cause pixel responses to differ. The resulting input voltages to the comparator, vC1 and vC2 are given by: vC1 = vS1 + vTh1 − vTr1 and vC2 = vS2 + vTh2 − vTr2, as produced by the comparator trim block, which makes use of capacitor switching to apply the

2012 JINST 7 C08001

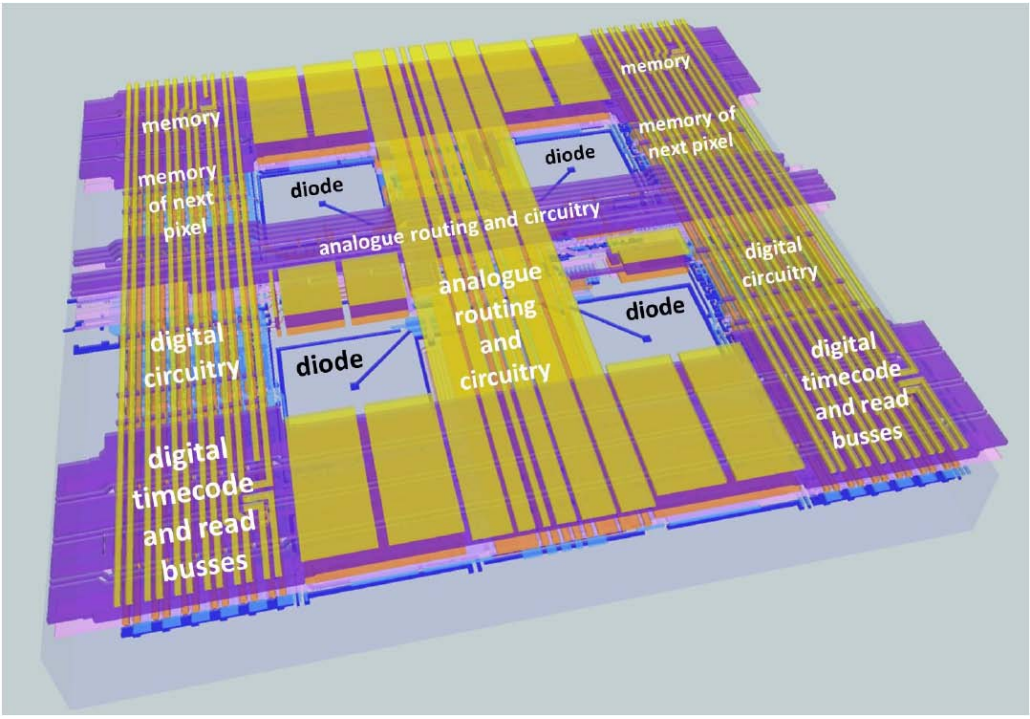

Figure 3. PImMS1 pixel layout.

global threshold and local trim voltages as shifts to the shaper pulses. A hit is signalled when the voltage at the comparator's inverting input (vC1) exceeds the voltage at its non-inverting input (vC2), as seen in the plot of vC in figure 2 — in other words, when the hit size, adjusted for local trim, exceeds the global threshold: $\mathrm{vS1} - \mathrm{vS2} + (\mathrm{vTr1} - \mathrm{vTr2}) > (\mathrm{vTh1} - \mathrm{vTh2})$.

The calibration process used to determine the appropriate trim value to apply to each pixel is described in section 4.

In addition to the four trim bits, each pixel also contains a masking bit used for disabling the writing of timecodes to the pixel's registers. This is useful for masking noisy pixels and is also used during sensor calibration.

The pixel layout is shown in figure 3, showing the separation between analogue and digital circuitry and routing, designed to minimise possible noise injection from the noisier digital busses into the analogue circuitry.

An important design choice for the sensor was the question of how many registers to include in each pixel. During a typical TOF-MS experiment, later, heavier ions may arrive at the same location as earlier ions. Having only a single timestamp register in a pixel would mean that a pixel that had recorded a timestamp would be blind to any subsequent ion strikes, potentially losing significant mass spectrum information. We simulated a number of representative arrival patterns of ions and concluded that within the typical statistics of a TOF-MS experiment, four registers are sufficient to obtain good ion detection efficiency [5], while still allowing the circuitry to fit within our target pixel size of $70 \times 70\,\mu\mathrm{m}^2$.

2012 JINST 7 C08001

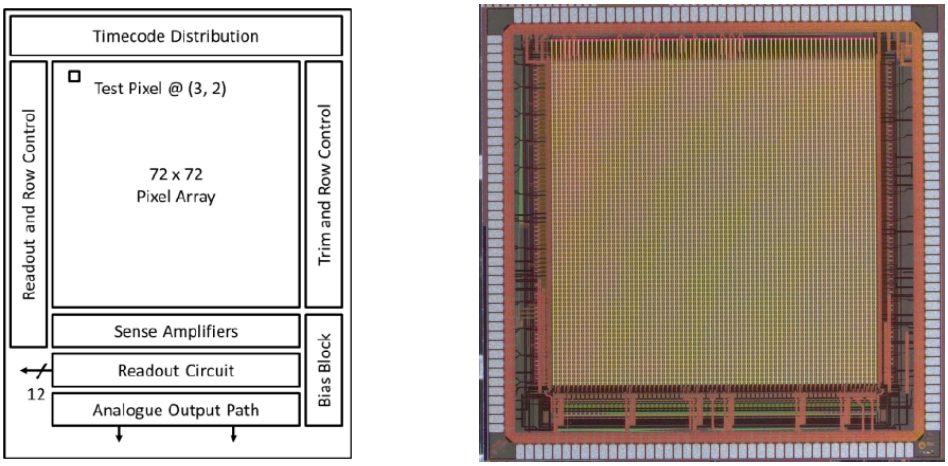

Figure 4. Left: PImMS1 sensor block diagram. Right: photo of PImMS1 sensor.

Time-stamping of ion events in this way requires in-pixel processing, but results in a relatively small amount of data to be read out from the sensor compared with framing approaches; the readout consists of an (x,y,t) data point for each detected ion rather than a large number of entire frames. An event counting sensor also has the advantage over a framing sensor that no prior information is needed on the expected ion arrival times when carrying out an experiment.

The front-end of the PImMS1 pixel design was adapted from a previous design for the Tera-Pixel Active Calorimeter (TPAC) family of sensors [8].

In total, the PImMS1 pixel contains over 600 transistors, both PMOS and NMOS. The technology that made it possible to include this amount of processing circuitry in each pixel is the Isolated N-Well Monolithic Active Pixel Sensor (INMAPS) process, developed at the Rutherford Appleton Laboratory [9]. The process includes a deep P-well implant to shield PMOS transistors, avoiding parasitic charge collection. This permits full CMOS circuits to be included inside imaging pixels without reducing charge collection efficiency. PImMS1 was designed on a 0.18 μm INMAPS process.

2.2 Sensor design

A block diagram of the PImMS1 sensor design is shown in figure 4. The sensor consists of an array of 72x72 pixels, each measuring $70\times70\,\mu\text{m}^2$, supported by configuration and readout circuitry arranged around the periphery of the array. The left edge contains row addressing and circuitry to shift the per-pixel configuration bits (mask and trim) into the array, while the right edge contains a readback of the configuration bits from the array. The top edge distributes the 12-bit global timecode throughout the array and also contains some bias distribution. The bottom edge contains readout circuitry, described further in the next section, and further bias distribution.

The array, as shown in figure 4, includes a test pixel which provides access to the analogue voltages on internal nodes after the shaper and before the comparator (i.e. once the pixel's trim offset has been applied).

2012 JINST 7 C08001

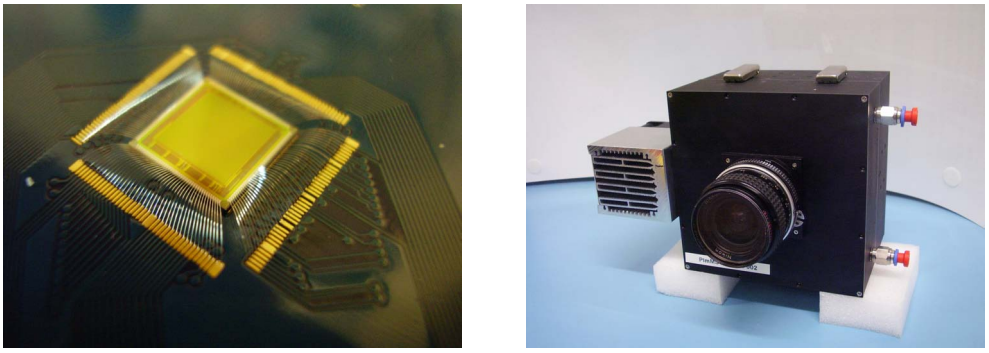

Figure 5. Left: photo of PImMS1 sensor, wire-bonded. Right: photo of PImMS1 camera.

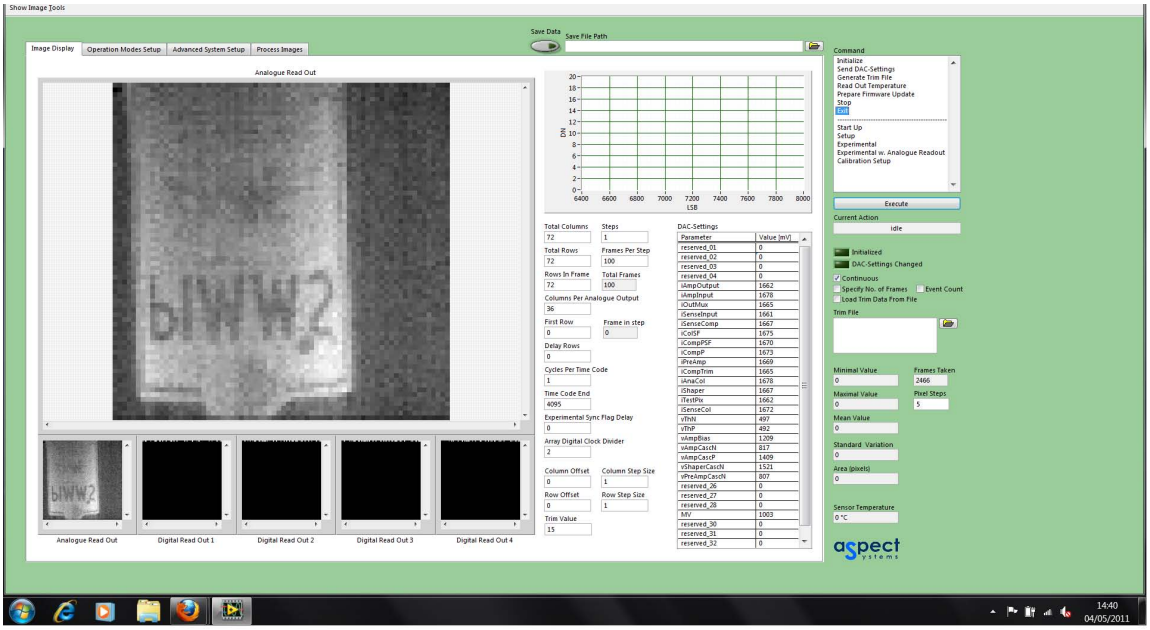

Figure 6. Sample analogue image taken with PImMS1.

3 PImMS1 sensor readout

The PImMS1 camera, shown in figure 5, houses the sensor and provides it with power and various voltage and current biases. It also furnishes sequences of control signals to ready and configure the sensor, capture experimental data and read out the sensor [10]. The camera is read out over a USB2 interface by a PC running the PImMS software application, written in LabVIEW. Features include configuration, calibration and readout of the sensor, as well as online and offline visualisation of the data. Figure 6 shows the software during analogue readout. A second software application, the PImMS Post-Processing Suite, adds further capabilities for visualising and processing mass spectrometry data, including display of mass spectrum and time intersections, time windowing, noisy pixel filtering and centroiding of clusters [11].

2012 JINST 7 C08001

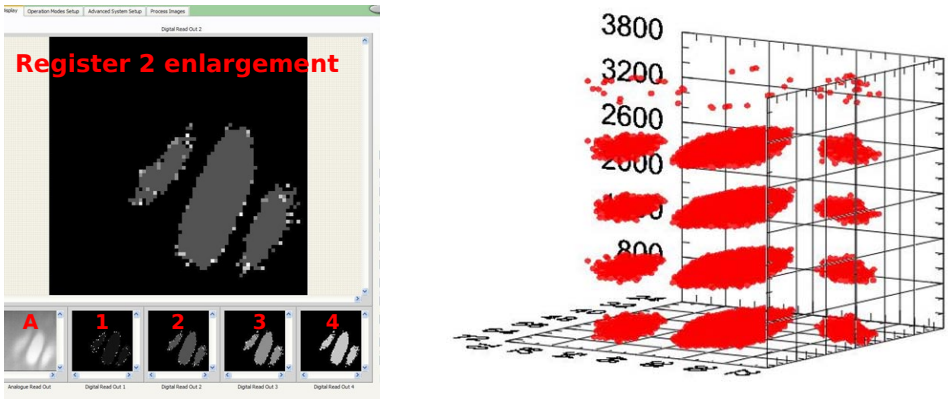

Figure 7. Left: readout image of 5 laser shots. Right: 3D visualisation of the 5 laser shot.

The sensor can be read in analogue mode, presenting an integrated grey-scale intensity image. This is used to focus the optical lens of the camera, as shown in a sample image in figure 6. In analogue readout, each pixel returns an analogue voltage corresponding to the output of the preamplifier (as shown in figure 2). This voltage represents the accumulated charge of the diodes integrated over time, i.e. the sum of any hits present and the effect of the leakage current, which accumulates during the experimental period and readout. The analogue readout circuitry is implemented using a pair of capacitors for each column which are alternately charged then read out and amplified. The camera implements a rolling shutter readout to equalise the integration time for all rows and digitises the analogue readout to a 14-bit digital number for transfer to a computer.

The main readout mode for the sensor is the digital readout of the pixels' timestamp registers. From an application point of view, the data is stored in this format: (*x, y, t, n_frame, n_register*), where *n_frame* is a sequence number for iterated experiments, and *n_register* is the register number (1–4) [11]. During experimental conditions, the majority of pixels are not expected to receive signal. Pixels which do not record hits are excluded from the data storage to disc, significantly reducing the size of the stored data sets. The readout circuitry of the sensor is implemented by sense amplifiers which read one register of one row at a time, for all columns in parallel, storing the read bits in a shift register along the bottom edge of the chip. A complete readout cycle iterates for each row and each of four registers, sensing the register contents, then shifting out the data on a 12-bit bus. The digital data read for one experimental cycle total 248832 bits. When performing experiments in a loop with the PImMS1 camera, allowing for sensor set-up time, the experimental period and readout time, experiments can be repeated at up to 550 Hz in practice.

Figure 7 shows a representative image of digital readout, taken when the sensor was stimulated by 5 shots of a laser which produced a pattern of three ovoid spots. On the left is a screen capture of the combined analogue and digital readout, with the analogue image marked 'A' and the contents of pixel registers 1–4 shown as four numbered images. In the digital images, paler shades of grey indicate later timecodes. On the right is the same data viewed as a three-dimensional image, with time as the vertical axis. This shows the first four laser shots hitting most pixels, filling the four registers in the majority of cases. The fifth laser shot can be seen at the top of the graph, as a fringe around the laser spots. This occurs where some pixels were not hit by all four initial laser shots,

2012 JINST 7 C08001

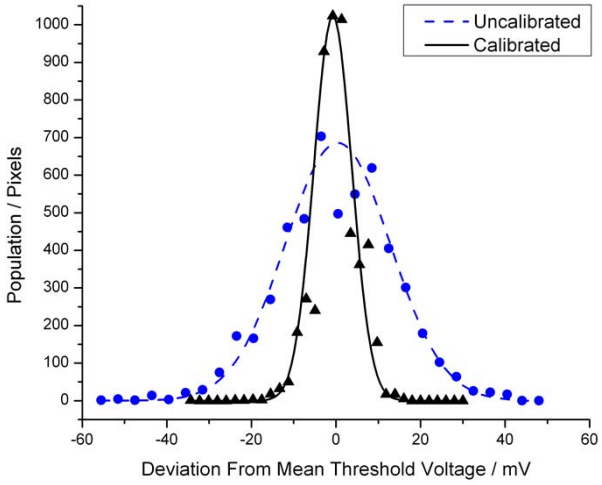

Figure 8. Deviation from mean threshold value before and after calibration.

due to reduced laser intensity at the outside of the spots, allowing the timecode of the fifth laser shot to be stored in those pixels.

4 PImMS1 sensor calibration

The sensor has a global threshold which is applied to all 5184 pixels. In addition, to account for differences in response of individual pixels, each pixel is capable of adjusting the threshold within a limited range, typically about 100 mV, with 4 trim bits allocated for the adjustment. The adjustment procedure (or calibration) aims at equalizing thresholds of all pixels to ensure uniform sensitivity of the sensor.

The first step in calibration is to determine the effective threshold of each pixel, initially using the same value of the trim register in all pixels. This is achieved by recording the number of hits in each pixel as a function of the common threshold. These threshold sweeps have a characteristic behaviour with zero occupancy for high threshold and a steep turn-on of the occupancy, which saturates at 4 times the number of cycles for low enough threshold due to the four registers available for storage in each pixel, as seen in the left image in figure 10. The plateau of hits seen on the right of the graph represents the hit behaviour at very low thresholds, where pixels are always in a hit state, and a single hit is recorded at the start of each experimental cycle.

The rising edge of each pixel is found to determine the initial response for each pixel. A correction is then applied using the trim register to shift the threshold as close as possible to a target value, common to all pixels in the sensor. Figure 8 shows deviations from mean threshold before and after calibration. The calibration procedure typically improves the standard deviation of pixel variation from 12.5 mV to 4.0 mV.

2012 JINST 7 C08001

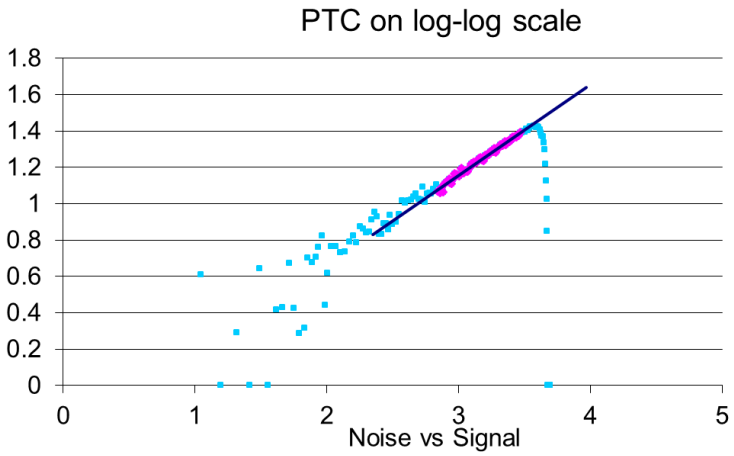

Figure 9. Photon Transfer Curve (PTC) on double logarithmic scale. The linear fit corresponds to the slope 0.5.

5 PImMS1 sensor characterisation

The PImMS1 sensor has been characterised optically using a technique known as Photon Transfer Curve (PTC) [12]. If a sensor is illuminated with a source of light, the signal follows the Poisson distribution with the RMS variation (or noise) equal to the square root of the signal. The relative variation (ratio of the RMS variation and signal) is independent of the signal units and therefore provides an absolute calibration and allows measurement of noise. When displayed on a log-log scale, as shown in figure 9, the dependence can be fit with a linear function with slope 0.5. The point on the graph with abrupt fall of the noise is reached at full well capacity for the charge collecting node and corresponds to about 24000 electrons. In the PImMS sensor, the analogue signal is only available after the preamplifier so the noise measured with this technique, 170 electrons, does not reflect the noise before the comparator. The sensor quantum efficiency was measured to be 7–9% for visible light using a calibrated light source. This agrees with expectations for the front illuminated sensor where openings in the top metal account only for about 17% of the area. Maximum sensitivity was achieved at 470 nm.

The sensor does not output the analogue information after the shaper, making the noise measurement at the comparator input less straightforward. Nevertheless the noise can be determined by looking at the dependence of the signal with respect to the threshold voltages applied in dark conditions. The left graph in figure 10 shows a threshold sweep for one of the pixels with the number of hits recorded with respect to a varying threshold. Each point is recorded over 50 experimental cycles to ensure a reliable statistical distribution. Lower voltage values correspond to a higher threshold on this plot. As the voltage values increase, the pixels begin to record signal. Further increase in voltage results in more counts which are followed by a drop and an eventual saturation at the total number of experimental cycles. Note that the maximum of the distribution can be more than the total cycle number as each pixel can record 4 hits per experimental cycle. The peak can be fitted to a Gaussian curve, the standard deviation of which corresponds to the sensor noise [13]. The right graph shows a typical distribution of the noise values for all pixels across a sensor, with a mean value of 3.9 mV. This is equivalent to 26 electrons noise based on simulation results.

2012 JINST 7 C08001

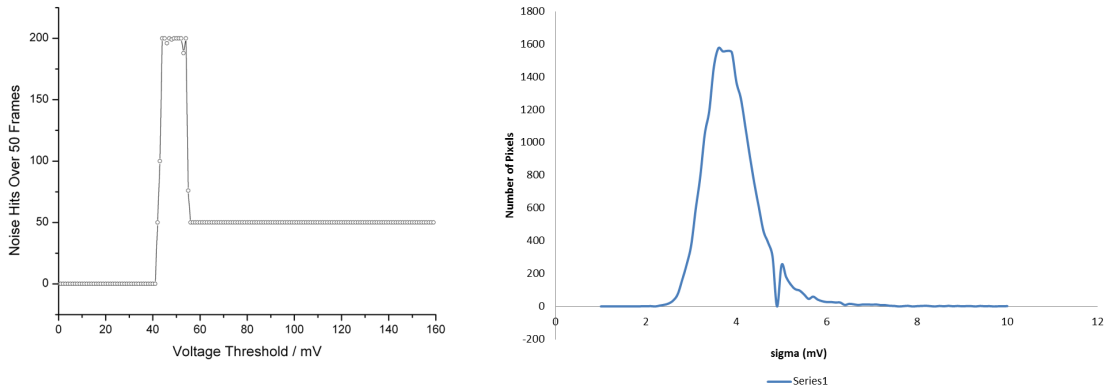

Figure 10. Left: threshold sweep for a typical pixel. Right: distribution of the noise values for all pixels in the sensor.

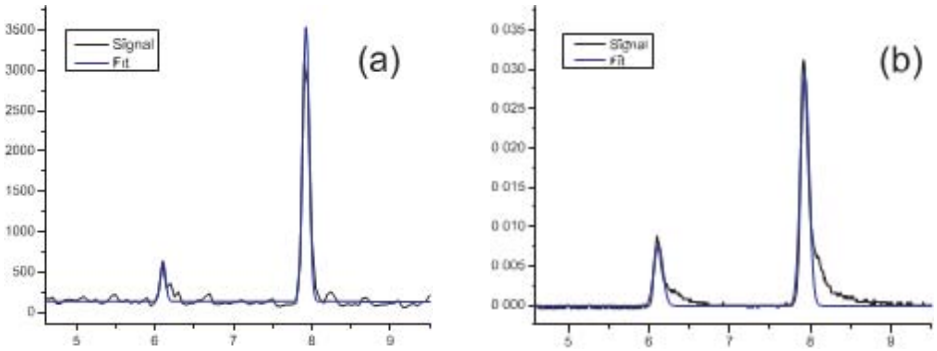

Figure 11. Comparison of mass spectra obtained with (a) PImMS1 and (b) a photomultiplier.

6 First PImMS1 application results

6.1 Imaging of α-cyano-4-hydroxycinnamic acid (CHCA) fragments

The PImMS1 camera was used to take first mass spectrometry data in the Department of Chemistry at the University of Oxford. A typical setup used for the measurements is described in detail in [14]. In all cases the position sensitive detector consisted of a pair of chevron microchannel plates coupled to a P47 phosphor screen, which has a decay lifetime of around 100 ns. The PImMS1 camera was used to acquire images of the bright spots generated on the phosphor for each incident ion.

Figure 11 compares time-of-flight spectra extracted from the data acquired (a) by the PImMS1 camera and (b) by a photomultiplier tube (PMT) positioned to record the total light intensity from the phosphor. The sample was α-cyano-4-hydroxycinnamic acid (CHCA), a commonly-used matrix for matrix-assisted laser desorption/ionization (MALDI) mass spectrometry, which gives rise to two clear peaks. The mass resolution of the system was limited by the phosphor decay lifetime which is clearly visible in the peak tails in (b). A Gaussian fit of the peaks in (a) gives a FWHM of about 90 ns, while (b) returns about 120 ns.

Figure 12 breaks down a data set similar to that used to construct the mass spectrum from figure 11 (a) into the signal components recorded in the first two registers of the PImMS1 sensor.

2012 JINST 7 C08001

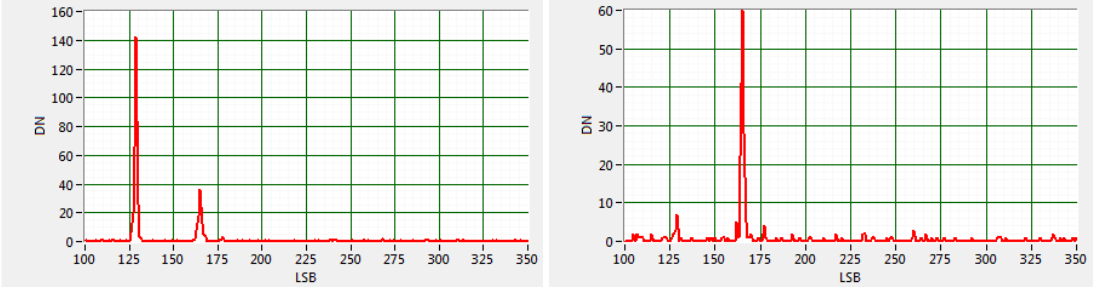

Figure 12. Mass spectra recorded with the first (left) and second (right) registers of PImMS1.

The left graph shows the number of pixels containing a given timecode in their first register, while the right graph shows the number of pixels containing a given timecode in their second register. In this experiment, the first mass peak observed was centred on timecode 127, while the second mass peak was centred on timecode 165. Note that the relative intensities of the two mass peaks are not directly comparable to those shown in figure 11, as they were taken under different experimental conditions.

As seen in the left graph in figure 12, the first mass peak at timecode 127 is almost entirely recorded in the pixels' first register as it represents the first major signal received by the detector. As the first peak and second peak at timecode 165 both originated from the same spatial position, hence arriving at the same pixels in many cases, the majority of the second signal is recorded in the pixels' second register as can be seen in the right graph in figure 12.

On the left, a smaller peak at timecode 165 can also be seen in the first register of some pixels. This represents the second mass striking pixels where the first ion was not recorded. On the right, a small amount of the first mass peak appears in the second register when some pixels registered background noise at earlier timecodes. The third and fourth registers, not shown here, contained only background noise for this experiment. The full time-of-flight mass spectrum is obtained from the sum of the time-of-flight spectra in the four different registers.

In summary, these results demonstrate the multi-hit capabilities of the PImMS1 sensor and show that it can be used for imaging of different masses within the same experimental cycle in the same pixels.

6.2 Imaging of the fragments arising from 193 nm photodissociation of carbon disulphide, CS_2

Here we present the results of imaging experiments in which the PImMS1 sensor was employed to study photodissociation of CS_2 molecules at 193 nm. Three projections of the full (x,y,t) data are shown in figure 13. The neutral CS_2 sample was prepared in a molecular beam, which flies along the time-of-flight axis. Absorption of a photon of 193 nm light leads to the formation of either the parent ion, CS_2^+, or CS^+ + S fragments. Loss of an electron has a minimal effect on the velocity of CS_2(the much lighter electron carries away virtually all of the excess energy following ionization), and the image from the parent ion therefore corresponds essentially to an image of the transverse velocity distribution of the molecular beam. This ion is visible as a small central point at late time in the images. In contrast, when the ion fragments to form CS^+, the available

2012 JINST 7 C08001

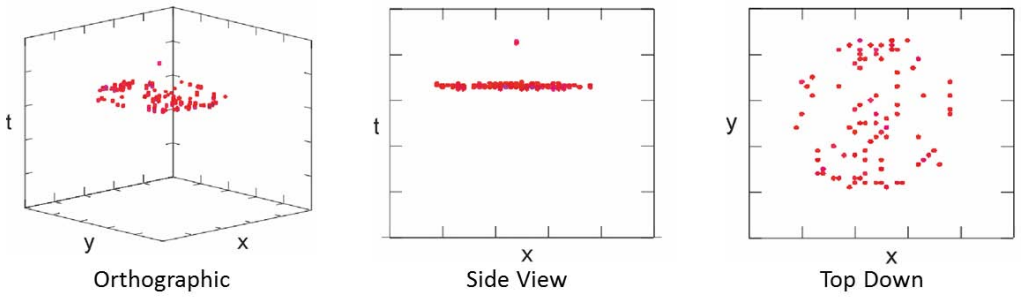

Figure 13. Different projections of imaged mass spectrum for the photodissociation of CS_2 obtained with PImMS.

energy (approximately equal to the photon energy less the bond dissociation energy of the C-S bond) is released into kinetic energy of the CS^+ and S fragments, and the resulting velocity-map image of the CS^+ ion shows a characteristic scattering distribution with a considerable velocity component in the transverse direction. The lighter CS^+ ions arrive at an earlier time-of-flight than the CS_2^+ parent ions. A number of velocity-map and spatial-map imaging experiments employing the PImMS1 camera are currently in progress.

7 PImMS2 sensor specifications

Following on from the PImMS1 sensor, we have designed a second-generation sensor to increase the imaging resolution. The next version of the sensor, PImMS2, will have 324×324 pixels with dimensions of $70\times70\,\mu m^2$ with the pixel and readout architecture remaining very similar to PImMS1. The new sensor will have 6 additional parallel digital outputs to reduce the readout time and a reduced pin count to facilitate interfacing in a vacuum. The reduced pin count is achieved by internal generation of current and voltage biases required for the sensor, as well as by adding counters to generate addresses and timecodes on-chip. The trim bias circuitry has been fine-tuned, which will lead to improved calibration. PImMS2 is expected to be received back from manufacturing in the second half of 2012.

8 Summary

We have described the design and first results from PimMS1, a novel monolithic CMOS sensor developed for applications in mass spectrometry. The sensor has been successfully characterised and tested for detection of low energy ions in time-of-flight mass spectrometers. The next generation sensor PImMS2 will be produced in 2012.

Acknowledgments

The support of the EPSRC through Grant EP/G00224X/1, of the STFC through PNPAS award, of the RC-U.K. through MI-3 programme (GR/S85733/01) and a 'proof of concept' grant from ISIS Innovation Ltd. are gratefully acknowledged. This work is protected in patents PCT/GB2008/004085 and PCT/GB2004/02014.

2012 JINST 7 C08001

References

[1] D.W. Chandler and P.L. Houston, *Two-dimensional imaging of state-selected photodissociation products detected by multiphoton ionization*, *J. Chem. Phys.* **87** (1987) 1445.

[2] A. Eppink and D.H. Parker, *Velocity map imaging of ions and electrons using electrostatic lenses: Application in photoelectron and photofragment ion imaging of molecular oxygen*, *Rev. Sci. Instrum.* **68** (1997) 3477.

[3] B.J. Whitaker ed., *Imaging in Molecular Dynamics*, Cambridge University Press, Cambridge U.K. (2003).

[4] A. Nomerotski et al., *Pixel Imaging Mass Spectrometry with fast silicon detectors*, *Nucl. Instrum. Meth.* **633** (2011) S243.

[5] A. Nomerotski et al., *Pixel Imaging Mass Spectrometry with fast and intelligent Pixel detectors*, 2010 *JINST* **5** C07007.

[6] M. Brouard, E.K. Campbell, A.J. Johnsen, C. Vallance, W.H. Yuen and A. Nomerotski, *Velocity map imaging in time of flight mass spectrometry*, *Rev. Sci. Instrum.* **79** (2008) 123115.

[7] D. Vu Truong Son et al., *Toward 100 Mega-Frames per Second: Design of an Ultimate Ultra-High-Speed Image Sensor*, *Sensors* **10** (2010) 16.

[8] J.A. Ballin et al., *Design and performance of a CMOS study sensor for a binary readout electromagnetic calorimeter*, 2011 *JINST* **6** P05009.

[9] J.A. Ballin et al., *Monolithic Active Pixel Sensors (MAPS) in a Quadruple Well Technology for Nearly 100% Fill Factor and Full CMOS Pixels*, *Sensors* **8** (2008) 5336.

[10] Aspect Systems GmbH, http://www.aspect-sys.com/.

[11] J.W.L. Lee, *PImMS Software Documentation v1.8*, project internal document, Oxford (July 2011).

[12] J.R. Janesick, *Photon Transfer: DN* $\rightarrow \lambda$, SPIE, Bellingham, U.S.A. (2007).

[13] A. Papoulis, *Probability, Random Variables and Stochastic Processes*, McGraw-Hill, New York (1984).

[14] W.S. Hopkins, M.L. Lipciuc, S.H. Gardiner and C. Vallance, *RG+ formation following photolysis of NO-RG via the A←X transition: a velocity-map imaging study*, *J. Chem. Phys.* **135** 034308 (2011).

2012 JINST 7 C08001